

Localization behavior in a Hermitian and non-Hermitian Raman lattice

Entong Zhao,¹ Yu-Jun Liu,¹ Ka Kwan Pak,¹ Peng Ren,² Mengbo Guo,¹ Chengdong He,² and Gyu-Boong Jo^{1,2}

¹*Department of Physics, The Hong Kong University of Science and Technology, Clear Water Bay, Kowloon, Hong Kong, China*

²*Department of Physics and Astronomy, Rice University, Houston, TX, USA*

We introduce a flexible Raman lattice system for alkaline-earth like atoms to investigate localization behaviors in a quasi-periodic lattice with controllable non-Hermiticity. We demonstrate that critical phases and mobility edges can arise by adjusting spin-dependence of the incommensurate potentials in the Hermitian regime. With non-Hermiticity introduced by spin-selective atom loss, we find the localization behaviour in this system can be suppressed by dissipation. Our work provides insights into interplay between quasi-periodicity and non-Hermitian physics, offering a new perspective on localization phenomena.

I. INTRODUCTION

In the presence of a disorder potential, quantum systems can exhibit exponential localization of wave functions induced by wave interference, a phenomenon known as Anderson localization [1]. Ultracold atom systems, with their exceptional purity and high controllability, enable detailed exploration of localization phenomena. Recent experiments have investigated Anderson localization in optical lattices with either random disorder [2] or incommensurate quasi-periodic structures [3–5].

For ultracold atoms, quasi-periodic optical lattices are created by superimposing two optical lattices with incommensurate wavelengths. In such setups, a notable transition from extended to localized states, commonly referred to as the Anderson transition, can manifest even within one-dimensional configurations [6, 7], contrary to uncorrelated disordered systems where such transitions are expected to occur only in dimensions higher than two according to the scaling theory [8, 9]. These systems also allow for the engineering of mobility edges-boundaries that separate coexisting localized and extended states at discrete energy levels [4, 10–14]. Recent theoretical studies suggest even more complex behavior, including intermediate critical phases and hybrid phases where localized, extended, and critical states coexist in specific one-dimensional quasi-periodic models [15, 16].

Recent years have seen growing interest in non-Hermitian physics [17, 18] across multiple research domains, including electrical circuits [19, 20], optics and photonics [21–24], optomechanics [25], NV centers [26, 27], trapped ions [28, 29], superconducting qubits [30] and ultracold atom systems [31–33]. Non-Hermitian systems display unique features such as exceptional points or rings [33–35], novel topological invariants, and the non-Hermitian skin effect [32, 36]. The Hatano-Nelson model, a fundamental non-Hermitian topological model, combines asymmetric hopping amplitudes with an on-site random potential [37]. However, a comprehensive understanding of the interplay between disorder and non-Hermiticity, particularly the influences of dissipation on localization behavior, remains largely unexplored [38–40].

Furthermore, experimental methods for studying this relationship between disorder and non-Hermiticity remain limited.

In this paper, we introduce a flexible Raman lattice scheme [41] tailored for ¹⁷³Yb atoms [42, 43] or alkaline-earth metal atoms [44] to investigate localization behaviors. The Raman lattice configuration induces quasi-periodicity using two optical lattices with incommensurate wavelengths, with the weak lattice potential akin to an incommensurate Zeeman potential. By adjusting the frequency of the incommensurate lattice close to the ¹S₀(*F* = 5/2) → ³P₁(*F* = 7/2) transition, the spin-dependent nature of the lattice potential may lead to the emergence of critical phases or mobility edges within the system. Finally, we generalize the Raman lattice with incommensurate potentials into the non-Hermitian regime with dissipation induced by atom loss [36]. The analysis reveals that dissipation exerts a significant influence on the localization behaviors within the system, offering a platform to investigate the intricate interplay between disorder potential and non-Hermitian physics.

The subsequent sections of this paper are structured as follows: Sec.II presents the model Hamiltonian of the flexible Raman lattice and outlines its experimental realization scheme. In Sec.III–V, we delve into the impact of the spin-dependency of the incommensurate lattice and dissipation within the system. Our focus will encompass three distinct scenarios: a completely spin-dependent incommensurate lattice, a partially spin-dependent incommensurate lattice, and an incommensurate lattice coupled with dissipation. Finally, Sec.VI offers a concise summary of the findings and conclusions derived from this investigation.

II. MODEL HAMILTONIAN

The Hamiltonian considered in this paper can be written as:

$$H = H_0 + \sum_{i,\sigma=\uparrow,\downarrow} (\delta_\sigma^i + i\gamma_\sigma) n_{i,\sigma} \quad (1)$$

where $\delta_\sigma^i = M_{z,\sigma} \cos(2\pi\beta i)$, with $M_{z,\sigma} \propto V_{s,\sigma}$ and γ_σ denotes the incommensurate Zeeman potential strength and dissipation strength for spin $\sigma = \uparrow, \downarrow$, respectively. $n_{i,\sigma} = c_{i,\sigma}^\dagger c_{i,\sigma}$ is the particle number operator, β is an irrational number and:

$$H_0 = -t_0 \sum_{i,\pm,\sigma} c_{i,\sigma}^\dagger c_{i\pm 1,\sigma} + t_{so} \sum_i \left[\left(c_{i,\uparrow}^\dagger c_{i+1,\downarrow} - c_{i,\downarrow}^\dagger c_{i-1,\uparrow} \right) + \text{H.c.} \right] \quad (2)$$

Here, t_0 (t_{so}) represents the spin-conserved (spin-flip) hopping strength between neighboring sites. The Hamiltonian renders a 1D AIII class topological insulator if replacing the incommensurate Zeeman potential with a constant uniform Zeeman potential [41, 42, 45, 46].

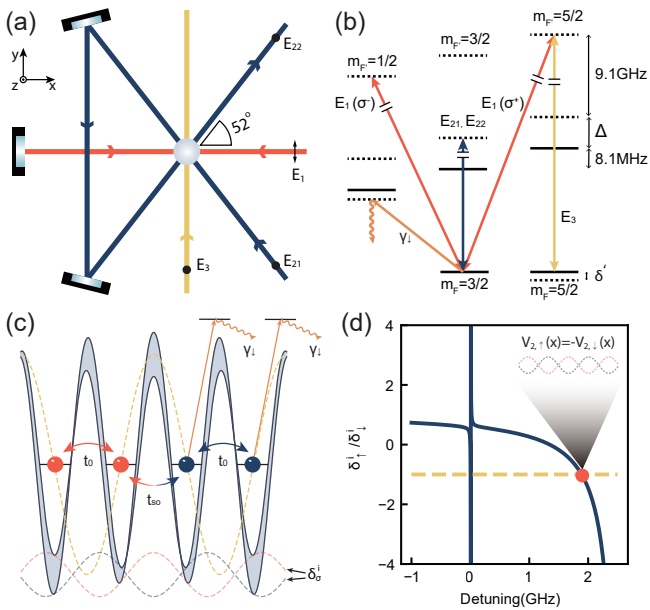


FIG. 1: **Experimental realization of critical phase in optical Raman lattice with ^{173}Yb atoms.** (a) Experimental setup of the optical Raman lattice consists of a standard 1D optical Raman lattice E_1 , E_3 with another spin-dependent incommensurate lattice E_{21} and E_{22} . (b) Schematic energy diagram with relevant transitions. (c) The incommensurate lattice induces a spin-dependent offset $V_{2,\sigma}(x)$ to the standard optical Raman lattice potential. (d) For the implementation of a perfect spin-dependent incommensurate lattice, the laser detuning should be set approximately 1.9 GHz blue-detuned from the $^1S_0(F = 5/2) \rightarrow ^3P_1(F = 7/2)$ transition.

This Hamiltonian can be experimentally implemented through the configuration outlined in Fig. 1(a). To establish the conventional optical Raman lattice potential [41, 42, 47], a standing-wave beam E_1 with y polarization and a free-running beam E_3 with z polarization are employed. The single-photon detuning of these two

beams can be finely tuned to approximately 11 GHz blue-detuned from the $^1S_0(F = 5/2) \rightarrow ^3P_1(F = 7/2)$ transition, as depicted in Fig. 1(b). In this setup, the primary lattice, characterized by a wave vector of $k_0 = 2\pi/\lambda$, exhibits nearly spin-independent lattice potential $V_{1,\sigma}(x) = V_{p,\sigma} \cos^2 k_0 x$ with $V_{p,\uparrow}/V_{p,\downarrow} \sim 1.01$, where $V_{p,\uparrow}/V_{p,\downarrow}$ denotes the primary lattice depth for spin up or spin down atoms. In the subsequent discussion, we will neglect the spin-dependent effects of the primary lattice potential ($V_{p,\uparrow} = V_{p,\downarrow} = V_p$). Moreover, two additional beams propagating at an angle of 52 degrees relative to the x direction are utilized to induce a spin-dependent incommensurate lattice featuring a wave vector of $k_1 = k_0 \cos \theta$, giving rise to a secondary incommensurate Zeeman potential $V_{2,\sigma} = V_{s,\sigma} \cos^2 k_1 x$ with $V_{s,\sigma}$ representing the incommensurate lattice depth, as illustrated in Fig. 1(c). The spin-dependence of this incommensurate lattice can be controlled through the detuning Δ of this lattice beam with respect to the $^1S_0(F = 5/2) \rightarrow ^3P_1(F = 7/2)$ transition. When $\Delta \sim 1.9$ GHz, the incommensurate lattice becomes entirely spin-dependent with $M_{z,\uparrow}/M_{z,\downarrow} = -1$ (Fig. 1(d)). To achieve a complete spin-independent configuration, the detuning of the incommensurate lattice can be set larger than 13GHz. The Raman coupling in this setup can be denoted by $\mathcal{M}(x) = M_R \cos k_0 x$. The introduction of dissipation into this Raman lattice setup can be realized through adding a nearly resonant loss beam with wavelength close to $^1S_0(F = 5/2) \rightarrow ^3P_1(F = 7/2)$ transition [36].

For simplicity, all phases along the y direction in these potentials are neglected during the calculation and the Hamiltonian governing this experimental setup can be expressed as:

$$H = \left[\frac{\hbar^2 k_x^2}{2m} + V_1(x) \right] \otimes \mathbf{1} + \sum_{\sigma=\uparrow,\downarrow} V_{2,\sigma}(x) |\sigma\rangle\langle\sigma| + \mathcal{M}(x) \sigma_x + \frac{\delta}{2} \sigma_z + \sum_{\sigma=\uparrow,\downarrow} \frac{i}{2} \gamma_\sigma |\sigma\rangle\langle\sigma| \quad (3)$$

Here, $\frac{\hbar^2 k_x^2}{2m}$ is the kinetic energy term and δ denotes the two-photon detuning. The incommensurate lattice introduces a weak spin-dependent energy offset characterized by the irrational number $\beta = \cos \theta \approx 0.6157$, where β is determined by the tilted angle. In our experimental configuration, which employs m_F states within the same hyperfine manifold as $|\uparrow, \downarrow\rangle$, the spin-dependence of the incommensurate lattice can be independently tuned by manipulating the detuning of the lattice beam, as it becomes challenging to simultaneously tune β and maintain a spin-dependent incommensurate lattice when β is determined by the ratio of the laser wavelength. This type of independent controllability of β and spin dependence of the incommensurate lattice broadens the range of choices for β . Notably, this contrasts with the methodology in [15], which requires two counter-propagating

lights with appropriate polarization and wavelengths approximating D1 and D2 lines in alkali-metal atoms, albeit unsuitable for alkaline-earth atoms such as Yb or Sr atoms [48].

III. LOCALIZATION BEHAVIOR IN THE HERMITIAN REGIME

Except for the localized phase, recent theoretical investigations have predicted the existence of a third fundamental phase, called critical phases, positioned between the localized and extended phases within such a spin-orbit coupled optical lattice featuring an incommensurate Zeeman potential [15, 36, 42]. Noteworthy features of these critical phases encompass critical spectral statistics [49–51], multifractal properties of wave functions [52–54], and dynamical evolutions [55–57]. Moreover, recent theoretical investigations have also unveiled the possibility of a quantum phase harboring coexisting localized, extended, and critical regions within a one-dimensional quasi-periodic model [16].

Therefore, we first consider an entirely spin-dependent incommensurate lattice ($M_{z,\uparrow}/M_{z,\downarrow} = -1$) in the Hermitian regime ($\gamma_\sigma = 0$), and find that a critical phase manifests in this configuration. The phase of this system can be characterized through the mean fractal dimension $\bar{\eta}$, as introduced by [15]:

$$\bar{\eta} = -\frac{\lim_{L \rightarrow \infty} \ln \left[(2L)^{-1} \sum_{m=1}^{2L} \sum_{j=1}^L (u_{m,j}^4 + v_{m,j}^4) \right]}{\ln 2L} \quad (4)$$

Here, $\bar{\eta}$ is averaged over all eigenstates, which can be represented as:

$$|\psi_m\rangle = \sum_{j=1}^L \left(u_{m,j} c_{j,\uparrow}^\dagger + v_{m,j} c_{j,\downarrow}^\dagger \right) |\text{vac}\rangle \quad (5)$$

It is established that, in extended (localized) states, the value of $\bar{\eta}$ tends towards 1 (0), while within the critical phase, $0 < \bar{\eta} < 1$.

In Fig.2(a), the mean fractal dimension is depicted as a function of M_z and t_{so} , revealing a distinct region where $0 < \bar{\eta} < 1$, indicating the emergence of the critical phase. The phase boundary can be delineated by $M_z = 2|t_0 \pm t_{so}|$, where the symbol + signifies the boundary between localization and critical phases, and – signifies the boundary between extended and critical phases [15]. Fig. 2(b) shows the fractal dimension for various eigenenergies and M_z when $t_{so} = 0.3$, illustrating that all individual states within the critical region exhibit critical behavior. However, if the incommensurate lattice is entirely spin-independent ($M_{z,\uparrow}/M_{z,\downarrow} = 1$), the critical phase region disappears, as illustrated in Fig. 2(c). Although a region where $\bar{\eta}$ deviates significantly from 1 and

0 can be identified, a further examination of the fractal dimension η of the corresponding eigenstates as a function of M_z suggests an intermediate regime characterized by the coexistence of extended and localized states rather than a critical phase (Fig.2(d)).

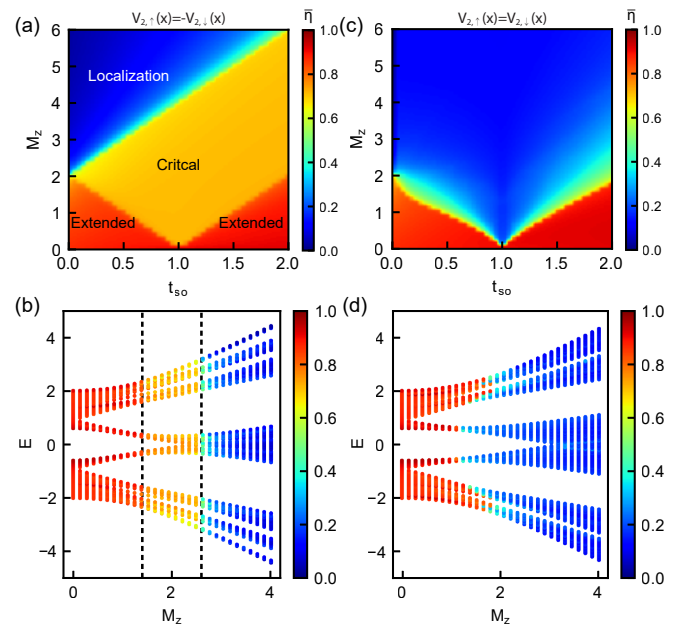


FIG. 2: **Phase diagram of the optical Raman lattice system with additional incommensurate lattice.** (a) The various phases, namely extended, critical, and localization phases, are distinguished based on the mean fractal dimension $\bar{\eta}$ when $M_{z,\uparrow}/M_{z,\downarrow} = -1$. M_z and t_{so} are presented in units of t_0 . (b) Fractal dimension η and energy of individual states for distinct values of M_z with $t_{so} = 0.3$ and $M_{z,\uparrow}/M_{z,\downarrow} = -1$. (c) Phase diagram of mean fractal dimension $\bar{\eta}$ as a function of M_z and t_{so} when $M_{z,\uparrow}/M_{z,\downarrow} = 1$. Other parameters are identical to those in b. (d) Fractal dimension η and energy of individual states for distinct values of M_z with $t_{so} = 0.3$ and $M_{z,\uparrow}/M_{z,\downarrow} = 1$. All results are simulated with $L = 1597$ and $\beta = 987/1597$ in periodic boundary condition.

In the pursuit of experimentally detecting localization behavior in an optical lattice system, one common method involves observing the expansion dynamics, as conducted in various studies [2–4]. Fig. 3(a) shows simulated time evolutions of wave packets positioned in the extended, critical, and localized phase regions. These simulations are based on an initial wave packet configuration defined as $|\psi_j(t=0)\rangle = (\sqrt{\pi}a)^{-1/2} e^{-(j-j_0)^2/2a^2} |\uparrow\rangle$, where a represents the half-width, and the packet is centered at site j_0 . Notably, the outcomes reveal distinctive behaviors: in the extended phase, the atom cloud exhibits ballistic expansion, while in the localized phase, occupancy remains predominantly restricted to the initial site. In the critical phase, a quasi-localization phenomenon is observed, with the atom cloud spreading to neighboring unit cells around the initial site, without

fully occupying the entire system.

To further characterize the expansion dynamics, the mean square displacement can be employed as an observable, defined as [15]:

$$W(t) = \left[\sum_{j,\sigma} (j - j_0)^2 \langle n_{j,\sigma}(t) \rangle \right]^{1/2} \quad (6)$$

In Fig.3(b), the evolution of W over time for various M_z values, with $a = 5$, is presented. In the extended phase, W rapidly converges to a large and stable value, while in the localized phase, W remains consistently small. Conversely, in the critical phase, W exhibits gradual and slow growth, distinguishing it from both the extended and localized regimes. Furthermore, the determination of phases can be facilitated by the time-averaged observable $\bar{W} = \frac{1}{N_t} \sum_{m=1}^{N_t} W(m\Delta T)$, where $N_t = 100$ and $\Delta t = 20$, representing the average width of the wave packet throughout the temporal evolution, as depicted in Fig. 3(c).

In most localization behavior studies, a crucial consideration lies in the necessity for the initial state to populate only a few lattice sites to ensure clarity in distinguishing between different phases (Fig.3(c)). While experimental setups in ultracold atom investigations enable the detection and preparation of Gaussian wavepackets as initial states through techniques like a matter wave magnifier[58, 59] or a quantum gas microscope [60–71], this can introduce complexity and inconvenience to the experimental arrangement. An intriguing observation emerges from numerical simulations represented in Fig. 3(a), indicating that in the extended phase, the presence of spin-down atoms is negligible when all initial states are occupied by spin-up atoms. Contrastingly, in the critical phase, clear evolution of spin-down atoms is observable over time. This can provide another way to detect the emergence of a critical phase in the current system.

In Fig.4(a), the spin polarization for systems where all lattice sites are initially uniformly occupied by spin up atoms is depicted for various phases. Within the extended phase, spin polarization exhibits minor oscillations with the value close to 1, while in critical and localized states, distinct oscillations occur, with the critical phase displaying larger oscillation amplitudes than the localized phase. Comparing with the distinct boundary between the extended and critical phases, the demarcation between the critical and localized phases, while not as pronounced, remains identifiable. Utilizing time-averaged spin polarization can aid in characterizing the emergence of the critical phase (Fig.3(c)-(d)). Notably, the time-averaged spin polarization tends towards zero in the critical phase, contrasting with higher values outside this phase.

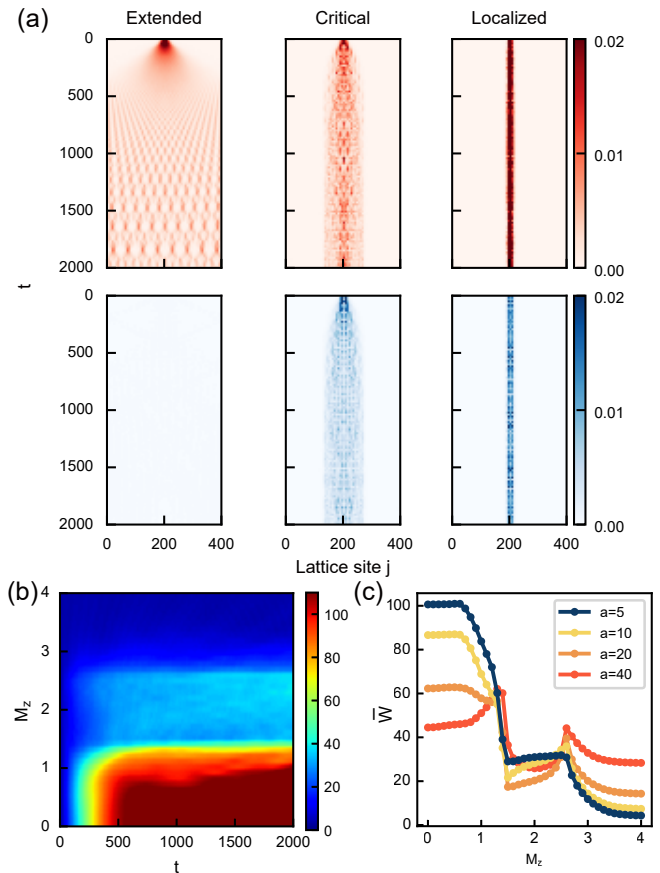


FIG. 3: **Simulation of detecting critical phase with expansion dynamics.** (a) Time evolution of the wave packet for the system located in the extended phase ($M_z = 0.5$), critical phase ($M_z = 2.0$), and localized phase ($M_z = 3.5$). (b) Expansion dynamics of the wave packet, characterized by W , as a function of M_z , with $t_{so} = 0.3$ and an initial width of $a = 5$. (c) Time-averaged \bar{W} as a function of M_z with different initial width a . All results are simulated with $L = 400$ and $\beta = \cos 52^\circ$ under open boundary condition.

IV. COEXISTENCE OF DIFFERENT STATES

Returning to the spin-independent incommensurate lattice case, although the critical phase is absent in such a system, under specific conditions, extended and localized states can coexist, separated by a mobility edge. For a more general situation, where the incommensurate Zeeman potential exhibits a blend of spin-dependence and independence, a phase emerges encompassing coexisting localized, extended, and critical regions [16]. Illustrated in Fig.5(a) is the fractal dimension corresponding to various eigenenergies and M_z , revealing regions where three or two distinct types of eigenstates coexist, separated by mobility edges. To validate the coexistence of difference phases within this domain, we consider the case of $M_z = 1.5$ as an example (refer to Fig.5(b)). Notably, as the system size increases, η converges towards 0 for all

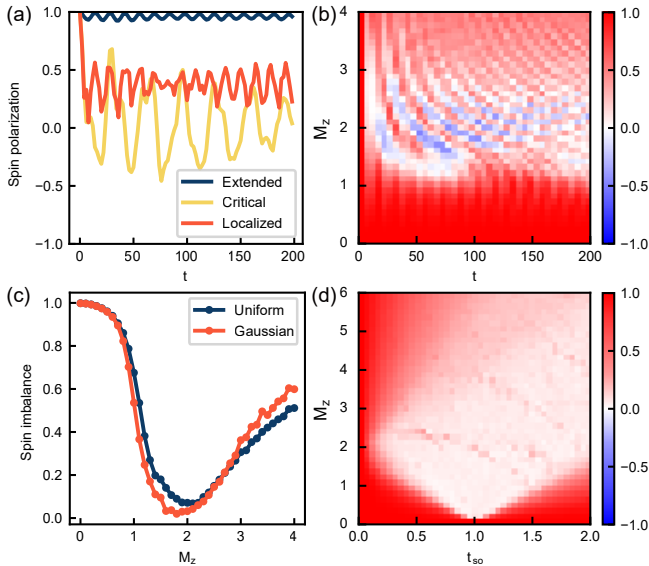


FIG. 4: **Evolution of spin polarization for different phases.** (a) Time evolution of the spin polarization for the system located in the extended phase ($M_z = 0.5$), critical phase ($M_z = 2.0$), and localized phase ($M_z = 3.5$) with the initial state comprising spin-up atoms in a uniform distribution. (b) Spin dynamics as a function of M_z , with $t_{so} = 0.3$, and an initial distribution in the spin up state uniform distribution. (c) Time-averaged spin polarization as a function of M_z averaged over $t = 0 - 200$ s, which show minimal disparity between initial states of uniform distribution or Gaussian distribution. (d) Time-averaged spin polarization as a function of M_z and t_{so} . All simulations are conducted with $L = 400$ and $\beta = \cos 52^\circ$ under open boundary conditions.

states in zones I and IV, indicative of localization states, while tending towards 1 for all states in zone III, signifying extended states. Conversely, within zones II and V, the fractal dimension markedly deviates from 0 and 1 and remains relatively constant with system size, suggesting a critical state in these regions.

The time evolution of the wave packet under such circumstances, as depicted in Fig.5(c), showcases characteristic signatures of these three distinct phases concurrently. On the whole, the time evolution of the wave packet exhibits quasi-localization, highlighting the presence of critical states. However, the higher concentration of atom clouds in the vicinity of central sites, particularly for spin-down atoms, indicates the existence of localized states. Furthermore, the inset of Fig.5(c) illustrates instances of ballistic expansion behavior of localized states upon closer inspection of the color bar. Through simulations of time evolution, the coexistence of extended, critical, and localized states under such conditions is further substantiated.

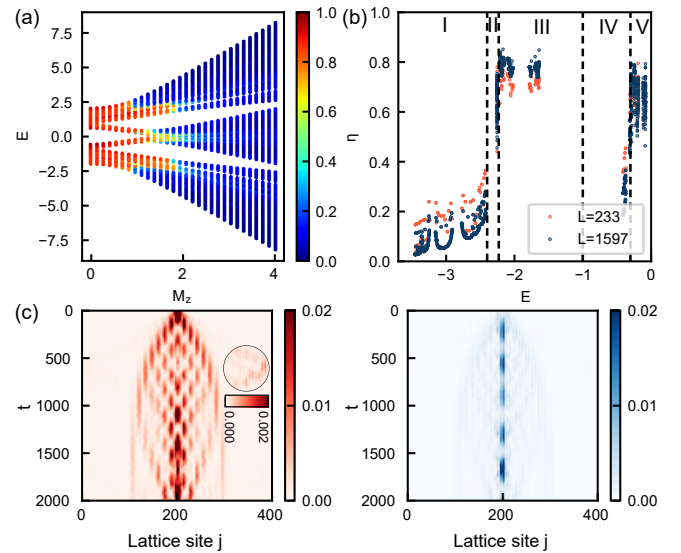


FIG. 5: **Phase with coexisting localized, extended, and critical zones.** (a) Fractal dimension η and energy of individual states for distinct values of M_z with $t_{so} = 0.3$ and $M_{z,\uparrow}/M_{z,\downarrow} = -2$ with $t_{so} = 0.3$. Simulations are conducted with $L = 1597$ and $\beta = 987/1597$ under periodic boundary condition. (b) Fractal dimension of different eigenstates as a function of eigenenergy for different system size $L = 233$ and $L = 1597$ with $M_z = 1.5$ and $t_{so} = 0.3$. For convenience, only the region with $E < 0$ is presented, which is symmetric to that with $E > 0$. (c) Time evolution of the wave packet for the system located in the phase with coexisting localized, extended, and critical zones ($M_z = 1.5$, $t_{so} = 0.3$ and $M_{z,\uparrow}/M_{z,\downarrow} = -2$). Simulations are conducted with $L = 400$ and $\beta = \cos 52^\circ$ under open boundary condition.

V. SUPPRESSION OF CRITICAL PHASE IN NON-HERMITIAN RAMAN LATTICE

Recently, various non-Hermitian extensions of systems exhibiting Anderson localization have been explored, such as the non-reciprocal Aubry-André model [72] and the PT-symmetric Aubry-André model [38, 40, 73–76]. Numerical studies have delved into the impact of non-reciprocal tunneling, physical gain and loss on parity-time symmetry breaking, the Hofstadter butterfly spectrum [40, 73, 74, 77], topological phase transitions [76], and the localization characteristics of eigenstates [37, 38, 72, 75, 78, 79]. Given these insights, it becomes pertinent to investigate the effects of non-Hermiticity on our system.

Expanding our setup into the non-Hermitian regime involves introducing dissipation to one of the spin states ($\gamma_\sigma \neq 0$) through a nearly resonant loss beam [79]. We focus on the scenario with $M_{z,\uparrow}/M_{z,\downarrow} = -1$, which exhibits a critical phase in the Hermitian context. The phase diagram for the system with dissipation ($\gamma_\downarrow = -2$) is illustrated in Fig. 6(a), revealing a transition of critical phases in the Hermitian regime to extended or localized

phases in non-Hermitian regime. Fig. 6(b) presents the mean fractal dimension $\bar{\eta}$ for varying dissipation values γ_{\downarrow} with $t_{so} = 1.0$. The plateau characterizing the critical phase in the Hermitian setup vanishes upon the introduction of dissipation. For system with larger M_z , the mean fractal dimension decreases, indicative of a transformation of eigenstates into localized states, whereas for lower M_z values, the mean fractal dimension rises, signifying a transition towards extended states.

Furthermore, Fig. 6(c) shows the fraction of eigenstates exhibiting different fractal dimensions, depicting a critical-extended transition. Employing a methodology akin to that in Fig. 5, it is observed that in the Hermitian regime, the fractal dimension remains stable, indicative of critical states in these regions. However, upon introducing dissipation ($\gamma_{\downarrow} = 2$), η converges towards 1 for all states when the system size increases, confirming the transformation of nearly all states into extended states and the suppression of the critical phase within the system due to the induced dissipation (Fig. 6(d)). This suppression of the critical phase is attributed to non-Hermiticity, as evidenced by the persistence of this effect even under conditions where $\gamma_{\uparrow}/\gamma_{\downarrow} = -1$.

VI. SUMMARY

This study introduces a versatile Raman lattice configuration aimed at investigating the localization behavior for alkaline-earth-like atoms, exemplified by ^{173}Yb . The experimental setup explores three distinct quasi-periodic Raman lattice configurations: an entirely spin-dependent incommensurate lattice in a Hermitian regime, a partially spin-dependent incommensurate lattice under Hermitian conditions, and a fully spin-dependent incommensurate lattice in a non-Hermitian regime. In the case of the entirely spin-dependent incommensurate lattice in the Hermitian regime, the emergence of a critical phase is observed, which can be detected by expansion dynamics and spin polarization evolution. Conversely, when the incommensurate lattice transitions into a combination of spin-dependent and spin-independent characteristics, a new phase with coexistence of extended, critical, and localized phases separated by mobility edges shows up. On the other hand, we also find that introducing dissipation into the system leads to the suppression of the critical phase due to non-Hermiticity within specific parameter spaces. This work aims to stimulate further experimental investigations into the interplay between the localization behavior and non-Hermiticity [72, 79] in ultracold atoms.

ACKNOWLEDGMENTS

GBJ acknowledges support from the RGC through 16306922, 16302123, 16305024, N-HKUST636-22, and

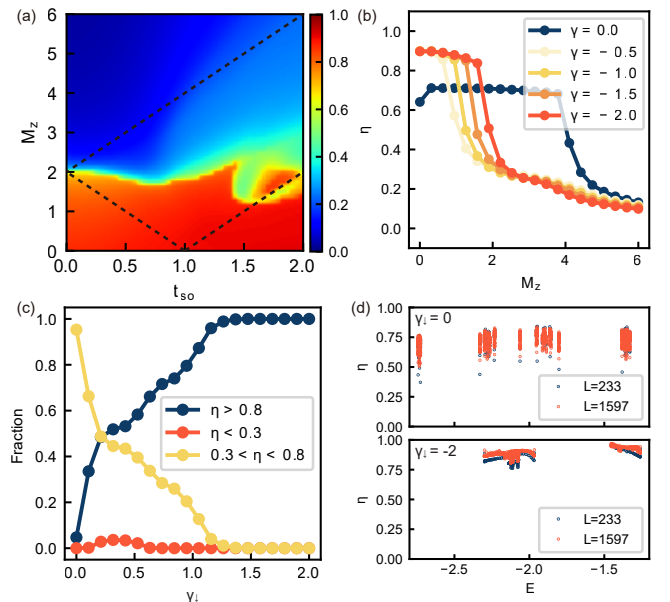


FIG. 6: Suppression of critical phase in non-Hermitian Raman lattice. (a) The phases diagram after inducing dissipation ($\gamma_{\downarrow} = -2$) to the system, distinguished based on the mean fractal dimension $\bar{\eta}$ when $M_{z,\uparrow}/M_{z,\downarrow} = -1$. M_z and t_{so} are presented in units of t_0 . The dashed lines show the boundary between different phases in Hermitian regime. (b) Mean fractal dimension $\bar{\eta}$ for different dissipation γ_{\downarrow} as a function of M_z with $t_{so} = 1.0$. (c) Fraction of eigenstates with $\eta > 0.8$, $\eta < 0.3$ and $0.3 < \eta < 0.8$ respectively as a function of γ_{\downarrow} with $t_{so} = 1.0$ and $M_z = 1.0$. (d) Fractal dimension of different eigenstates as a function of eigenenergy for different system size $L = 233$ and $L = 1597$ with $M_z = 1.5$ and $t_{so} = 0.3$. The top one is without dissipation and the bottom one is with dissipation. For convenience, only the region with $E < 0$ is presented, which is symmetric to that with $E > 0$. Unless otherwise specified, all simulations are conducted with $L = 1597$ and $\beta = 987/1597$ under periodic boundary condition.

RFS2122-6S04.

-
- [1] P. W. Anderson, Physical review **109**, 1492 (1958).
 - [2] J. Billy, V. Josse, Z. Zuo, A. Bernard, B. Hambrecht, P. Lugan, D. Clément, L. Sanchez-Palencia, P. Bouyer, and A. Aspect, Nature **453**, 891 (2008).
 - [3] G. Roati, C. D'Errico, L. Fallani, M. Fattori, C. Fort, M. Zaccanti, G. Modugno, M. Modugno, and M. Inguscio, Nature **453**, 895 (2008).
 - [4] H. P. Lüschen, S. Scherg, T. Kohlert, M. Schreiber, P. Bordia, X. Li, S. Das Sarma, and I. Bloch, Physical review letters **120**, 160404 (2018).
 - [5] T. Xiao, D. Xie, Z. Dong, T. Chen, W. Yi, and B. Yan, Science bulletin **66**, 2175 (2021).
 - [6] D. Grempel, S. Fishman, and R. Prange, Physical Review Letters **49**, 833 (1982).
 - [7] C. Aulbach, A. Wobst, G.-L. Ingold, P. Hänggi, and

- I. Varga, *New Journal of Physics* **6**, 70 (2004).
- [8] D. J. Thouless, *Physics Reports* **13**, 93 (1974).
- [9] E. Abrahams, P. W. Anderson, D. C. Licciardello, and T. V. Ramakrishnan, *Physical Review Letters* **42**, 673 (1979).
- [10] S. D. Sarma, S. He, and X. Xie, *Physical review letters* **61**, 2144 (1988).
- [11] F. Evers and A. D. Mirlin, *Reviews of Modern Physics* **80**, 1355 (2008).
- [12] J. Biddle and S. Das Sarma, *Physical review letters* **104**, 070601 (2010).
- [13] F. A. An, E. J. Meier, and B. Gadway, *Physical Review X* **8**, 031045 (2018).
- [14] F. A. An, K. Padavić, E. J. Meier, S. Hegde, S. Ganeshan, J. Pixley, S. Vishveshwara, and B. Gadway, *Physical review letters* **126**, 040603 (2021).
- [15] Y. Wang, L. Zhang, S. Niu, D. Yu, and X.-J. Liu, *Physical Review Letters* **125**, 073204 (2020).
- [16] Y. Wang, L. Zhang, W. Sun, T.-F. J. Poon, and X.-J. Liu, *Physical Review B* **106**, L140203 (2022).
- [17] R. El-Ganainy, K. G. Makris, M. Khajavikhan, Z. H. Musslimani, S. Rotter, and D. N. Christodoulides, *Nat.Phys* **14**, 11 (2018).
- [18] Y. Ashida, Z. Gong, and M. Ueda, *Advances in Physics* **69**, 249 (2021), ISSN 0001-8732, review article commissioned by *Advances in Physics* - 191 pages, 49 figures, 8 tables, 2006.01837, URL [arXiv.org](https://arxiv.org/abs/2006.01837).
- [19] T. Helbig, T. Hofmann, S. Imhof, M. Abdelghany, T. Kiessling, L. Molenkamp, C. Lee, A. Szameit, M. Greiter, and R. Thomale, *Nature Physics* **16**, 747 (2020).
- [20] M. Ezawa, *Physical Review B* **99**, 201411 (2019).
- [21] S.-B. Lee, J. Yang, S. Moon, S.-Y. Lee, J.-B. Shim, S. W. Kim, J.-H. Lee, and K. An, *Physical Review Letters* **103**, 134101 (2009), ISSN 0031-9007, 0905.4478.
- [22] L. Xiao, T. Deng, K. Wang, G. Zhu, Z. Wang, W. Yi, and P. Xue, *Nature Physics* **16**, 761 (2020).
- [23] H. Zhou, C. Peng, Y. Yoon, C. W. Hsu, K. A. Nelson, L. Fu, J. D. Joannopoulos, M. Soljačić, and B. Zhen, *Science* **359**, 1009 (2018).
- [24] S. Weidemann, M. Kremer, T. Helbig, T. Hofmann, A. Stegmaier, M. Greiter, R. Thomale, and A. Szameit, *Science* **368**, 311 (2020).
- [25] Y. S. S. Patil, J. Höller, P. A. Henry, C. Guria, Y. Zhang, L. Jiang, N. Kralj, N. Read, and J. G. E. Harris, *Nature* **607**, 271 (2022), ISSN 0028-0836, 2112.00157.
- [26] W. Zhang, X. Ouyang, X. Huang, X. Wang, H. Zhang, Y. Yu, X. Chang, Y. Liu, D.-L. Deng, and L.-M. Duan, *Physical Review Letters* **127**, 090501 (2021).
- [27] Y. Yu, L.-W. Yu, W. Zhang, H. Zhang, X. Ouyang, Y. Liu, D.-L. Deng, and L.-M. Duan, *npj Quantum Information* **8**, 116 (2022).
- [28] M.-M. Cao, K. Li, W.-D. Zhao, W.-X. Guo, B.-X. Qi, X.-Y. Chang, Z.-C. Zhou, Y. Xu, and L.-M. Duan, *Physical Review Letters* **130**, 163001 (2023).
- [29] Y. Zhang, J. Carrasquilla, and Y. B. Kim, *Nature Communications* **16**, 3286 (2025).
- [30] W. Chen, M. Abbasi, Y. N. Joglekar, and K. W. Murch, *Physical Review Letters* **127**, 140504 (2021).
- [31] J. Li, A. K. Harter, J. Liu, L. d. Melo, Y. N. Joglekar, and L. Luo, *Nature Communications* **10**, 855 (2019), 1608.05061.
- [32] Q. Liang, D. Xie, Z. Dong, H. Li, H. Li, B. Gadway, W. Yi, and B. Yan, *Physical review letters* **129**, 070401 (2022).
- [33] Z. Ren, D. Liu, E. Zhao, C. He, K. K. Pak, J. Li, and G.-B. Jo, *Nature Physics* **18**, 385 (2022).
- [34] B. Zhen, C. W. Hsu, Y. Igarashi, L. Lu, I. Kaminer, A. Pick, S.-L. Chua, J. D. Joannopoulos, and M. Soljačić, *Nature* **525**, 354 (2015).
- [35] Y.-J. Liu, K. K. Pak, P. Ren, M. Guo, E. Zhao, C. He, and G.-B. Jo (2025), 2412.17705, URL <https://arxiv.org/abs/2412.17705>.
- [36] E. Zhao, Z. Wang, C. He, T. F. J. Poon, K. K. Pak, Y.-J. Liu, P. Ren, X.-J. Liu, and G.-B. Jo, *Nature* **637**, 565 (2025).
- [37] N. Hatano and D. R. Nelson, *Physical review letters* **77**, 570 (1996).
- [38] Q.-B. Zeng, S. Chen, and R. Lü, *Physical Review A* **95**, 062118 (2017).
- [39] D.-W. Zhang, L.-Z. Tang, L.-J. Lang, H. Yan, and S.-L. Zhu, *Science China Physics, Mechanics & Astronomy* **63**, 267062 (2020).
- [40] A. K. Harter, T. E. Lee, and Y. N. Joglekar, *Physical Review A* **93**, 062101 (2016).
- [41] X.-J. Liu, Z.-X. Liu, and M. Cheng, *Physical review letters* **110**, 076401 (2013).
- [42] B. Song, L. Zhang, C. He, T. F. J. Poon, E. Hajiyev, S. Zhang, X.-J. Liu, and G.-B. Jo, *Science advances* **4**, eaao4748 (2018).
- [43] B. Song, C. He, S. Niu, L. Zhang, Z. Ren, X.-J. Liu, and G.-B. Jo, *Nature Physics* **15**, 911 (2019), 16 pages including supplementary material, 4 figures, 1808.07428, URL [arXiv.org](https://arxiv.org/abs/1808.07428).
- [44] M.-C. Liang, Y.-D. Wei, L. Zhang, X.-J. Wang, H. Zhang, W.-W. Wang, W. Qi, X.-J. Liu, and X. Zhang, *Physical Research* **5**, L012006 (2023), 2109.08885.
- [45] B.-Z. Wang, Y.-H. Lu, W. Sun, S. Chen, Y. Deng, and X.-J. Liu, *Physical Review A* **97**, 011605 (2018).
- [46] L. Zhang and X.-J. Liu, in *Synthetic Spin-Orbit Coupling in Cold Atoms* (World Scientific, 2018), pp. 1–87.
- [47] Z. Wu, L. Zhang, W. Sun, X.-T. Xu, B.-Z. Wang, S.-C. Ji, Y. Deng, S. Chen, X.-J. Liu, and J.-W. Pan, *Science* **354**, 83 (2016), 27 pages, 5 figures.
- [48] C. He, E. Hajiyev, Z. Ren, B. Song, and G.-B. Jo, *Journal of Physics B: Atomic, Molecular and Optical Physics* **52**, 102001 (2019).
- [49] T. Geisel, R. Ketzmerick, and G. Petschel, *Physical review letters* **66**, 1651 (1991).
- [50] K. Machida and M. Fujita, *Physical Review B* **34**, 7367 (1986).
- [51] C. L. Bertrand and A. M. García-García, *Physical Review B* **94**, 144201 (2016).
- [52] T. C. Halsey, M. H. Jensen, L. P. Kadanoff, I. Procaccia, and B. I. Shraiman, *Physical review A* **33**, 1141 (1986).
- [53] A. D. Mirlin, Y. V. Fyodorov, A. Mildenerger, and F. Evers, *Physical review letters* **97**, 046803 (2006).
- [54] R. Dubertrand, I. García-Mata, B. Georgeot, O. Giraud, G. Lemarié, and J. Martin, *Physical Review Letters* **112**, 234101 (2014).
- [55] H. Hisashi and A. Shuji, *Journal of the Physical Society of Japan* **57**, 1365 (1988).
- [56] R. Ketzmerick, K. Kruse, S. Kraut, and T. Geisel, *Physical review letters* **79**, 1959 (1997).
- [57] M. Larcher, F. Dalfovo, and M. Modugno, *Physical Review A* **80**, 053606 (2009).
- [58] P. Murthy, D. Kedar, T. Lompe, M. Neidig, M. Ries, A. Wenz, G. Zürn, and S. Jochim, *Physical Review A* **90**, 043611 (2014).

- [59] L. Asteria, H. P. Zahn, M. N. Kosch, K. Sengstock, and C. Weitenberg, *Nature* **599**, 571 (2021).
- [60] W. S. Bakr, J. I. Gillen, A. Peng, S. Fölling, and M. Greiner, *Nature* **462**, 74 (2009).
- [61] J. F. Sherson, C. Weitenberg, M. Endres, M. Cheneau, I. Bloch, and S. Kuhr, *Nature* **467**, 68 (2010).
- [62] M. Miranda, R. Inoue, Y. Okuyama, A. Nakamoto, and M. Kozuma, *Physical Review A* **91**, 063414 (2015).
- [63] E. Haller, J. Hudson, A. Kelly, D. A. Cotta, B. Peaudecerf, G. D. Bruce, and S. Kuhr, *Nature Physics* **11**, 738 (2015).
- [64] G. J. Edge, R. Anderson, D. Jervis, D. C. McKay, R. Day, S. Trotzky, and J. H. Thywissen, *Physical Review A* **92**, 063406 (2015).
- [65] A. Omran, M. Boll, T. A. Hilker, K. Kleinlein, G. Salomon, I. Bloch, and C. Gross, *Physical review letters* **115**, 263001 (2015).
- [66] L. W. Cheuk, M. A. Nichols, K. R. Lawrence, M. Okan, H. Zhang, and M. W. Zwierlein, *Physical review letters* **116**, 235301 (2016).
- [67] M. F. Parsons, A. Mazurenko, C. S. Chiu, G. Ji, D. Greif, and M. Greiner, *Science* **353**, 1253 (2016).
- [68] R. Yamamoto, J. Kobayashi, T. Kuno, K. Kato, and Y. Takahashi, *New Journal of Physics* **18**, 023016 (2016).
- [69] D. Mitra, P. T. Brown, E. Guardado-Sanchez, S. S. Kondov, T. Devakul, D. A. Huse, P. Schauß, and W. S. Bakr, *Nature Physics* **14**, 173 (2018).
- [70] R. Yamamoto, H. Ozawa, D. C. Nak, I. Nakamura, and T. Fukuhara, *New Journal of Physics* **22**, 123028 (2020).
- [71] K. Kwon, K. Kim, J. Hur, S. Huh, and J.-y. Choi, *Physical Review A* **105**, 033323 (2022).
- [72] H. Jiang, L.-J. Lang, C. Yang, S.-L. Zhu, and S. Chen, *Physical Review B* **100**, 054301 (2019), ISSN 2469-9950.
- [73] C. Yuce, *Physics Letters A* **378**, 2024 (2014).
- [74] C. H. Liang, D. D. Scott, and Y. N. Joglekar, *Physical Review A* **89**, 030102 (2014).
- [75] C. Hang, Y. V. Kartashov, G. Huang, and V. V. Konotop, *Optics letters* **40**, 2758 (2015).
- [76] S. Longhi, *Physical review letters* **122**, 237601 (2019).
- [77] S. Longhi, *Journal of Physics A: Mathematical and Theoretical* **47**, 165302 (2014), URL <https://dx.doi.org/10.1088/1751-8113/47/16/165302>.
- [78] N. M. Shnerb and D. R. Nelson, *Physical review letters* **80**, 5172 (1998).
- [79] L. Zhou, *Physical Review B* **108**, 014202 (2023).